Smart Ward Control Based on a Wearable Multimodal Brain–Computer Interface Mouse

Junbiao Zhu, Kendi Li, *Graduate Student Member, IEEE*, Sicong Chen, Haiyun Huang, *Member, IEEE*, Yupeng Zhang, Li Hu, and Yuanqing Li, *Fellow, IEEE*

***Abstract*— For patients with severe extremity motor function impairment, traditional smart ward control methods, such as those using joysticks and touchscreens, are frequently unsuitable due to their limited physical abilities. Consequently, developing an effective brain–computer interface (BCI) suitable for their operation has become an immediate concern. This paper presents a wearable multimodal BCI system for smart ward control, which employs a self-designed wearable headband to capture head rotation and blinking movement. By wearing the headband, users can control a computer cursor on the screen only with head rotation and blinking, and further control devices in a smart ward with self-designed graphical user interfaces (GUIs). The system decodes signals from an inertial measurement unit (IMU) to map the head posture to the position of the cursor on the screen and decodes electrooculography (EOG) and electroencephalography (EEG) signals to detect valid blinks for selecting and activating function buttons. Ten participants were recruited to perform two experimental tasks that simulate the daily needs of patients with extremity motor function issues. To our satisfaction, all the participants fully accomplished the simulated tasks, and an average accuracy of 97.0 ± 3.9 % and an average response time of 2.39 ± 0.53 s were achieved. Different from traditional step-controlled BCI nursing beds, we designed a continuous-controlled nursing bed and achieved satisfactory results. Furthermore, workload evaluation using NASA Task Load Index (NASA-TLX) revealed that the participants experienced a low workload when using the system. The experimental results demonstrate the effectiveness of our proposed system, indicating significant potential for practical applications.**

***Index Terms*— Brain–computer interface (BCI), head posture, multimodal, smart ward control, wearable device.**

I. Introduction

In THE 2020s, human–computer interaction (HCI) systems have permeated every aspect of our lives. These systems enable users to interact with external devices in an efficient manner to accomplish various tasks. Commonly used HCI methods include touchscreens [1], gesture recognition [2], virtual reality (VR) [3], augmented reality (AR) [4], speech interaction [5], and etc. However, some patients with severe extremity motor function impairment, such as those suffering from stroke, spinal cord injuries (SCI), and amyotrophic lateral sclerosis (ALS), are unable to use these conventional HCI methods to interact with external devices. These patients typically experience partial or complete loss of body function, affecting motor and sensory functions. Therefore, assistive devices and systems are needed to help them perform daily activities independently to improve their quality of life.

Many researchers have now directed their efforts towards developing effective HCI methods for people with mobility issues in upper and lower extremities to realize independent operation of external devices without extremity engagement [6], [7], [8], [9]. Researchers have attempted to address this issue using various physiological signals, such as electroencephalography (EEG) [10], [11], [12], electromyography (EMG) [13], and electrooculography (EOG) [14], [15]. Among them, EEG has received extensive attention currently. For example, an event-related potential (ERP) brain–computer interface (BCI)-based environmental control system was proposed, which integrates household appliances, nursing beds, and smart wheelchairs [16]. The system was evaluated for SCI patients, and the results showed that the system has

Received 21 April 2025; revised 11 November 2025; accepted 6 January 2026. Date of publication 12 January 2026; date of current version 23 January 2026. This work was supported in part by the Brain Science and Brain-Like Intelligence Technology-National Science and Technology Major Project under Grant 2022ZD0208900; in part by the Key Research and Development Program of Guangdong Province, China, under Grant 2018B030339001; and in part by the National Natural Science Foundation of China under Grant 62306120 and Grant 82401739. *(Corresponding authors: Li Hu; Yuanqing Li.)*

This work involved human subjects or animals in its research. Approval of all ethical and experimental procedures and protocols was granted by the Ethics Committee of Guangdong Provincial Work Injury Rehabilitation Hospital, China, under Application No. AF/SC-07/2023.02.

Junbiao Zhu and Yupeng Zhang are with the School of Automation Science and Engineering, South China University of Technology, Guangzhou 510640, China, and also with South China Brain-Computer Interface Technology Company Ltd., Guangzhou 510320, China.

Kendi Li, Sicong Chen, and Yuanqing Li are with the School of Automation Science and Engineering, South China University of Technology, Guangzhou 510640, China, also with the Research Center for Brain-Computer Interfaces, Pazhou Laboratory, Guangzhou 510330, China, and also with South China Brain-Computer Interface Technology Company Ltd., Guangzhou 510320, China (e-mail: auyqli@scut.edu.cn).

Haiyun Huang is with the School of Artificial Intelligence, South China Normal University, Foshan 528225, China.

Li Hu is with the School of Electronic and Information, Guangdong Polytechnic Normal University, Guangzhou 510665, China, and also with South China Brain-Computer Interface Technology Company Ltd., Guangzhou 510320, China (e-mail: huli@gpnu.edu.cn).

Digital Object Identifier 10.1109/TNSRE.2026.3653138

great potential in helping severely paralyzed patients improve their self-care abilities. Similarly, a daily assistance system for ALS patients based on a wearable BCI was proposed and showed promising long-term application prospects [17]. Some researchers developed a BCI-based living environment adjustment system, using single-channel EEG to monitor cognitive state changes for automatically adjusting living environment [18]. A color-timed BCI was proposed to help patients with SCI control a nursing bed robot using motor imagery (MI) EEG [19]. Controlling external devices by decoding users' EEG signals offers the advantages of directness and high personalization. Despite the promising experimental results, a literature review revealed that most applications of BCI assistive systems have focused on proposing methodology [20], neglecting its usability in daily care scenarios [21]. Most EEG-based BCI systems cost a large amount of money, which is not affordable for ordinary people. Besides, the control efficiency of these systems is often limited, and users require extensive training to use it effectively. In addition, studies have shown that simplicity is the key to broader acceptance of BCI assistive systems [22], [23], [24]. Most EEG devices are not portable, uncomfortable to wear, and complicated to operate. These limitations restrict their application among patients with extremity motor function issues [25], [26]. We're in pursuit of low-cost and portable assistive HCI systems without a complicated training process.

To solve this problem, some researchers have developed affordable and portable systems to assist patients in daily activities. Using an eye tracker to control external devices is a convenient assistance method. An eye-tracking-based adjustable electric nursing bed control system was proposed for patients with severe physical limitations, which aimed at improving their self-care abilities and quality of life [27]. Some researchers experimented with an eye-tracking-based device controller to help users control household devices [28]. A monocular head-free 3D gaze tracking technology was applied to an electric hospital bed to help patients with limited mobility adjust their bed posture [29]. However, the performance of these devices is limited by several environmental conditions, such as indoor lighting conditions, so they may be ineffective in outdoor environments [30]. Infrared eye trackers are highly sensitive to ambient lighting, and video eye trackers demand high computational power and are limited by the scope of the scene. At the same time, the cost and complexity of eye-tracking devices are also limitations for their application in HCI. In response to these limitations, EOG-based control has emerged as a promising alternative for assistive HCI, with many researchers exploring its potential in device control. Researchers have used EOG to develop text input systems [31] and intelligent wheelchairs systems [32], which achieved satisfactory performance in terms of accuracy and user acceptance. However, distinguishing between voluntary and involuntary blinks remains a key challenge for EOG-based assistive systems, as involuntary physiological blinks can easily lead to false triggers and reduce system reliability. Recent studies have achieved preliminary success in EEG-based attention recognition, such as Liu et al.'s work with an offline accuracy of 76.82% [33], which can support the reliable detection of valid blinks. It is crucial to develop an assistance system for patients that is affordable, easy to use, and not limited by environmental conditions.

In this study, we developed a wearable multimodal BCI system to help patients with extremity motor function impairment control various devices in a smart ward without relying on neuromuscular function. It employs a self-designed wearable headband to capture blinking signals and head posture. By wearing the headband, users can control a computer cursor on the screen with head rotation and eye blinking, and further control external devices in a smart ward with self-designed graphical user interfaces (GUIs). The system decodes gyroscope data to map the head posture to the position of the cursor on the screen and decodes EOG and EEG signals to detect valid blinks for selecting and activating function buttons. We establish a smart ward environment and design two experimental tasks that simulate the daily needs of patients with extremity motor function issues. To our satisfaction, all 10 participants fully accomplished the simulated tasks, and an average accuracy of 97.0% and an average response time of 2.39 s were achieved in the smart ward control task. Different from traditional step-controlled BCI nursing beds, we designed a continuous-controlled nursing bed and achieved satisfactory results. During idle state testing, the system did not produce any false triggers. Furthermore, workload evaluation using NASA Task Load Index (NASA-TLX) revealed that the participants experienced a low workload when using the system. The experimental results demonstrate the effectiveness of our proposed system, indicating the significant potential of this wearable multimodal BCI system for practical applications.

The remainder of this article is organized as follows. Section II explains the materials and methods, including the participants, the equipment, the GUI, the paradigm, and some backgrounds; Section III describes the detailed experimental results; Section IV evaluates and discusses the proposed method; Section V concludes the article and provides prospects for future research.

II. Materials and Methods

In this study, we propose a wearable multimodal BCI for smart ward control. By wearing a wearable headband, users can move a cursor and select functional buttons on the tablet with head rotation and eye blinking. They can further control a smart ward using a self-designed GUI.

A. Participants

Ten healthy Chinese participants (4 females and 6 males, aged 24 to 43 years) were recruited for this study. All participants were right-handed, with normal head motor function and eye function, and no history of eye diseases. None of the participants had a history of psychiatric, neurological, or other brain-related disorders. The study was approved by the Ethics Committee of Guangdong Provincial Work Injury Rehabilitation Hospital, China. Informed consent was obtained from all participants before the study, ensuring they fully understood its purpose and procedures. Among the participants, 4 had prior experience with the BCI used in this study, while the remaining 6 were first-time users.

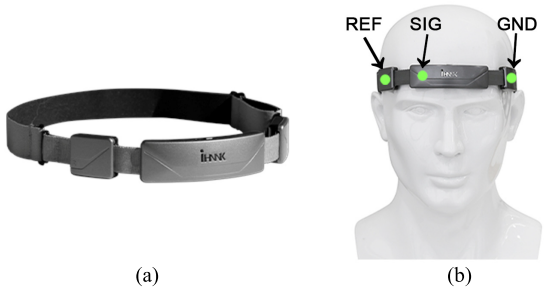

Fig. 1. (a) The wearable headband and (b) its wearing position and electrode position.

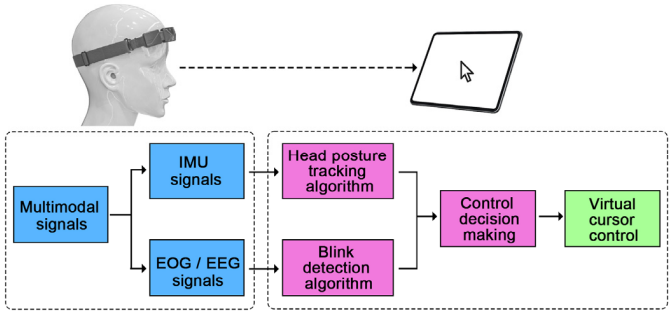

Fig. 2. Framework of the BCI mouse system.

B. Signal Acquisition

In this system, we employed a self-designed wearable headband for head posture tracking blink detection, as shown in Fig. 1 (a). The headband consists of 3D-printed plastic components, hydrogel electrodes, and an elastic strap. The plastic components are used to secure the electrodes and hardware circuits, while the elastic strap forms an adjustable closed loop to accommodate different head shapes. As shown in Fig. 1 (b), the EOG and EEG signals were recorded with three hydrogel electrodes in shape with a diameter of 16 mm. The reference electrode and the ground electrode were placed at the user's left and right temples, marked as "GND" and "REF". The signal electrode was positioned on user's forehead, marked as "SIG". The contact impedance of all electrodes with the skin was maintained below 5kΩ. The recorded signals were then processed using a self-designed wearable amplifier (for more details, please refer to [34] and [35]). The sampling frequency for the signals was set to 250 Hz.

Head posture tracking was achieved using a 9-axis inertial measurement unit (IMU), which operated at a sampling frequency of 50 Hz. To perform data alignment, EEG and EOG signals, IMU signals, event markers, and electrode impedances were all systematically numbered. The wireless communication module employed BLE 5.0 technology to transmit data wirelessly to a tablet for real-time visualization, analysis, and storage.

C. BCI Mouse System

Fig. 2 presents the framework of the BCI mouse system. By wearing the headband, users can control a virtual cursor on the screen only with head rotation and eye blinking. Specifically, users moved the cursor up, down, left, or right by turning the head up, down, left, or right, respectively. The cursor click was accomplished through a single eye blink. Therefore, if users intended to click a button, they first moved the cursor to the button by head rotation, and then performed a single eye blink for the cursor click. If the cursor clicking movement responses inadequately, the user can navigate to the calibration GUI and follow the on-screen instructions to calibrate, enhancing the precision of blink recognition. During the calibration, users are guided to blink gently every 2 s and repeat 10 times.

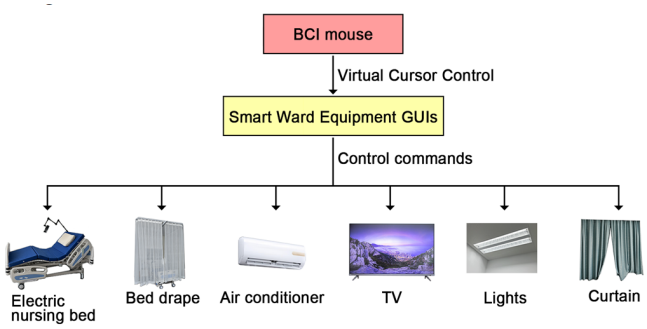

Fig. 3. Framework of the smart ward system based on the BCI mouse.

D. Smart Ward Control Based on the BCI Mouse

The smart ward system is further designed based on the BCI mouse system, and the framework is presented in Fig. 3. By wearing the wireless headband, users can move a cursor and select functional buttons on a tablet with head rotation and eye blinking. They can further control a smart ward using a self-designed GUI.

1) Equipment: We built a smart ward environment according to the daily needs of patients with extremity motor function issues. Referring to the configuration of hospital wards, we designed a smart ward of 3.5 m in width and 6 m in length. It is equipped with an electric nursing bed, bed drapes, an air conditioner, a television, lights, curtains. All 6 devices can be wirelessly controlled by the proposed system. The tablet analyzes multimodal signals for virtual cursor control and provides control instructions, which are sent to the electric nursing bed control module, bed drape control module, air conditioning control module, lighting control module, television control module, and curtain control module for smart ward control.

2) GUIs and Control Strategies: When the user correctly wears the headband and lies down on the electric nursing bed, they can initiate the system and access the system control GUI. First, the cursor is invisible on the screen, and the user must activate it by speaking out "Unlock cursor". With the cursor activated, the users controlled a cursor on the screen with slight head rotation and eye blinking.

Fig. 4 illustrates the wearable multimodal BCI, which features a dual-layer GUI. The first layer serves as the system switch GUI (as shown in Fig. 4 (a)), primarily facilitating the activation and exit of the system. The second layer is the main menu GUI (as shown in Fig. 4 (b)), topped with three buttons that direct users to the calibration GUI, the smart ward GUIs, and system switch GUI. The smart ward

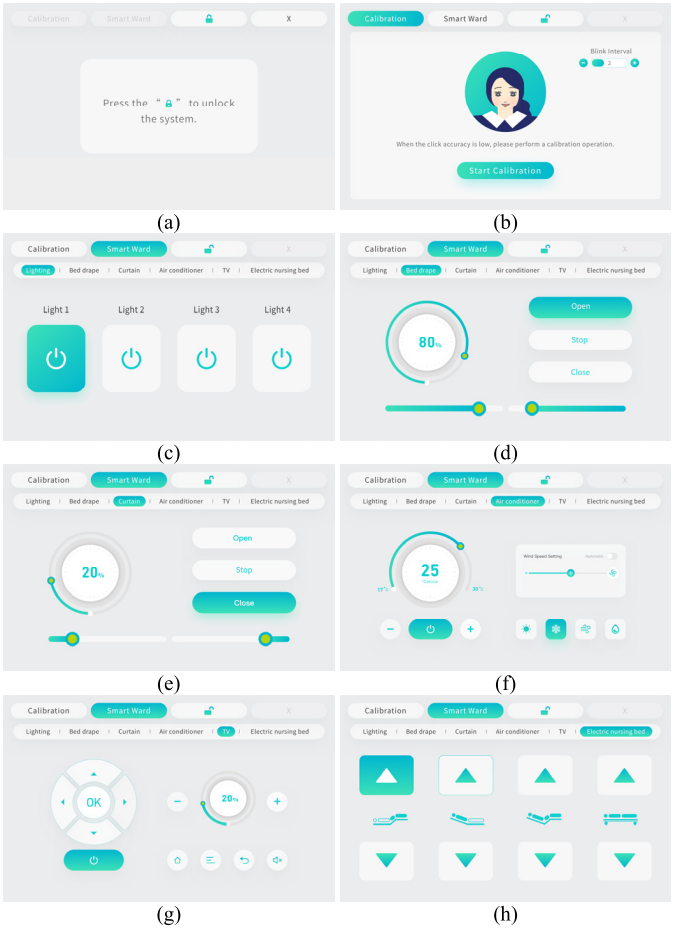

Fig. 4. GUIs of the smart ward system. (a) System switch GUI, (b) calibration GUI, (c) light control GUI, (d) bed drape control GUI, (e) curtain control GUI, (f) air conditioner control GUI, (g) TV control GUI, and (h) electric nursing bed control GUI.

GUIs include 6 functional GUIs (as shown in Fig. 4 (c)-(h)), which are lighting control, bed drape control, curtain control, air conditioning control, TV control, and electric nursing bed control, respectively. Each GUI is outfitted with multiple buttons with icons that correspond to the respective functions, which helps users recognize and comprehend the function of each button.

In the electric nursing bed control GUI in Fig. 4 (h), there are eight function buttons: raise backrest, lower backrest, raise leg rest, lower leg rest, simultaneously raise backrest and leg rest, simultaneously lower backrest and leg rest, raise bed, and lower bed. Users can execute the desired actions by clicking these buttons. Different from the other devices, the electric nursing bed operates on a control logic simulating the hand-controlled electric nursing bed, where pressing and holding the button the bed to move continuously, and releasing the button stops the bed. When a user clicks a function button in electric nursing bed GUI, they keep the cursor within the button area for continuous movement. The movement will stop as soon as the cursor is moved out of this area. Operations for other devices in the ward are executed by single-clicking their respective buttons. To operate the same button again, the user must first move the cursor out of the button area, then move

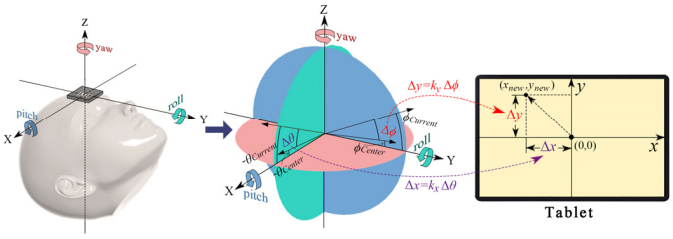

Fig. 5. Principle of transformation of head posture and cursor position.

it back and click. For instance, to switch the lights from off to on and back to off, the user must move the cursor out of the switch button area, reposition it, and then click the switch button while blinking to turn off the light.

E. Signal Analysis

The system realized cursor movement and clicking by detecting users' head rotation and blinking. This process involves the analysis of IMU signals, EOG and EEG signals.

1) Head Posture Tracking: Head posture tracking was achieved using a 9-axis IMU, incorporating a 3-axis gyroscope, a 3-axis accelerometer, and a 3-axis magnetometer. As depicted in Fig. 5, the system employs a 32-bit ARM Cortex M4 processor as its microcontroller (MCU). It collects data from the IMU at a sampling rate of 50Hz and uses this data to calculate the orientation angles of the head along the X, Y and Z axes. These angles are denoted by θ, ϕ, and ψ, corresponding to rotations around the Y, X and Z axes, respectively. The reference coordinate system uses a right-handed coordinate system. In this coordinate system, the positive direction of rotation around each axis is determined by the right-hand rule. The angle is positive when rotating in the positive direction. Conversely, if the direction of rotation is opposite to the positive direction, the angle is negative. The roll angle (θ) is used to control the horizontal movement of the cursor on the screen, while the pitch angle (ϕ) is used to control the vertical movement. The reference position when the user's head is aligned with the screen is set as the initial zero point for the cursor, with the roll angle θ_{center} and the pitch angle $\phi_{current}$. In the initial state, the zero point of the cursor is set at the center of the screen, where the horizontal midline and vertical midline intersect.

Next, we calculate the differences between the current head roll angle ($\theta_{current}$) and pitch angle ($\phi_{current}$) and their respective zero points (θ_{center} and ϕ_{center}), which are denoted as $\Delta\theta$ and $\Delta\phi$ respectively. As depicted in Fig. 5, the changes in the pitch angle and roll angle are subsequently converted into the cursor's displacement in the x-direction (Δx) and y-direction (Δy) respectively, as follows:

$$\Delta x = k_x \Delta\theta \tag{1}$$

$$\Delta y = k_y \Delta\phi \tag{2}$$

Finally, we update the cursor's position. (x_0, y_0) are the original coordinates $(0, 0)$, (x_{new}, y_{new}) represents the updated coordinates, with the updating formulas:

$$x_{new} = x_0 + \Delta x \tag{3}$$

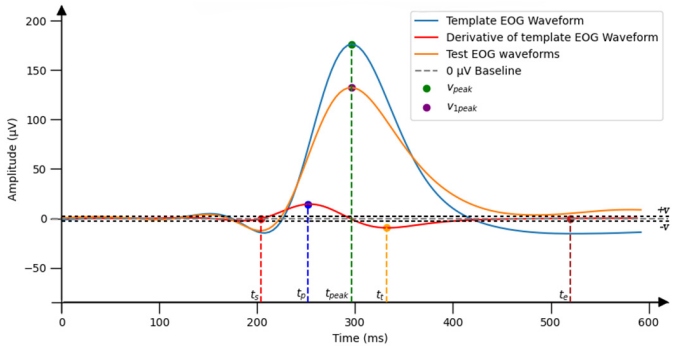

Fig. 6. Example of EOG data processing during blinking detection.

$$y_{new} = y_0 + \Delta y \tag{4}$$

Note that the range of head rotation for users lying on the electric nursing bed varies individually, where healthy users generally have a wider range than patients with various conditions. Such variations can be addressed via manual adjustment of the scaling factors k_x and k_y to adjust sensitivity, thus making the system applicable to all users with basic neck movement ability. Additionally, an anti-jitter algorithm is integrated to filter out involuntary minor head tremors, thus preventing unintended cursor movements.

2) Blinking Detection: Signals collected at "SIG" electrode are processed to detect blinking movement. User's EOG signals are continuously acquired and stored. Upon the cursor hovering over a target button for a duration of 300 ms, the system starts a blinking detection algorithm to identify the user's blinking actions. The algorithm is executed every 100 ms, during which the system intercepts a passing 600-ms segment of the raw EOG signal (600 ms $\times$250Hz = 150 sampling points). The system then subtracts the average value of the first 100 ms of this segment to perform baseline correction. Subsequently, a 10th-order infinite impulse response (IIR) filter is applied for bandpass filtering between 0.1 Hz and 10 Hz. Following this filtration, the system identifies peaks within the EOG signal and constructs a preprocessed waveform consisting of 149 data points, centered on the peak, with 74 data points each from before and after the peak. Once a valid blink is detected, the algorithm is deactivated. To ensure phase alignment between the preprocessed EOG waveform and the calibrated template EOG waveform, the peaks of both waveforms are used as reference points for alignment. As depicted in Fig. 6, $f_1(t)$ denotes the preprocessed EOG waveform, with v_{1peak} indicating its peak; $f(t)$ represents the processed EOG template waveform during calibration, with v_{peak} as its peak at time t_{peak}. $f'(t)$ is the first derivative of the template EOG waveform, where t_p and t_t denote the times of the peak and trough, respectively. The start time (t_s) and end time (t_e) of the blink action are calculated using the following formulas:

$$t_s = \underset{t_i}{\text{argmax}} \left\{ 0 \le f'(t_i) \le v \text{ and } t_i \le t_p \right\} \tag{5}$$

$$t_e = \underset{t_i}{\text{argmin}} \left\{ -v \le f'(t_i) \le 0 \text{ and } t_i \ge t_t \right\} \tag{6}$$

where t_i the time corresponding to the i-th data point, and v is the threshold value, which is set to $v = 1$ in this case.

To mitigate the impact of noise beyond blinking actions, we isolated segments of the template and preprocessed EOG waveforms spanning from t_s to t_e. We then assessed the resemblance between these two waveform segments by determining their Pearson correlation coefficient. The calculation is detailed as follows:

$$r = \frac{\sum_{t_s}^{t_e} (f(t) - \bar{f}) \left(f_1(t) - \overline{f_1}\right)}{\sqrt{\sum_{t_s}^{t_e} (f(t) - \bar{f})^2} \sqrt{\sum_{t_s}^{t_e} \left(f_1(t) - \overline{f_1}\right)^2}} \tag{7}$$

In the equation mentioned above, $\overline{f}$ denotes the time-averaged value of $f(t)$ over the blinking duration, whereas $\overline{f}_1$ signifies the time-averaged value of $f_1(t)$ over the same interval.

The energies of $f(t)$ and $f_1(t)$ between t_s and t_e are then calculated separately as follows:

$$E_f = \sum_{t_s}^{t_e} \left[f(t) \right]^2 \tag{8}$$

$$E_{f_1} = \sum_{t_s}^{t_e} \left[f_1(t) \right]^2 \tag{9}$$

Finally, the presence of a blink motion is determined using the following thresholds:

$$blink = \begin{cases} 1, & if\ (r > r_{min}) \\ & \cap \left(E_{f_1} > \varepsilon E_f\right) \\ 0, & otherwise \end{cases} \tag{10}$$

where, r_{min} denotes the Pearson correlation coefficient threshold. εE_f denotes the energy threshold, and ε is the energy threshold coefficient.

In addition, we carried out attention detection using the collected EEG signals to distinguish between attentive and inattentive states, aiming to minimize false clicks caused by involuntary blinking. Relevant studies have reported an association between β and θ band activity in the prefrontal cortex and attention states [36], [37], [38], [39]. Based on this finding, several attention-based systems using single-channel prefrontal EEG have been proposed [40], [41]. Accordingly, we adopted the spectral ratio between β (13-30 Hz) wave power and θ (4)-8 Hz) wave power of EEG signals as the metric of the attention level. A time window of 5 s with a stride of 100 ms (consistent to EOG processing) was employed to cut continuous signals into signal epochs. We then extracted power spectral density (PSD) features from the signal epoch, similar to the method used in our previous studies [42], [43], [44]. A short-time Fourier transform (STFT) was performed to obtain spectral points within β and θ waves. The spectral ratio between the sum of β spectral points and the sum of θ spectral points was calculated and used as the metric of the attention level. A higher attention level corresponded to a greater value of the spectral ratio. As this metric is varying among individuals, the decision threshold was dynamically adjusted during use [45], [46], [47]. The decision threshold was set at 70% of the average of the spectral ratios in the last 30 s. When the spectral ratio fell below this threshold, it indicated that the participant was in non-attentional state. Note that attention detection was only activated in the electric nursing bed control to prevent misoperations.

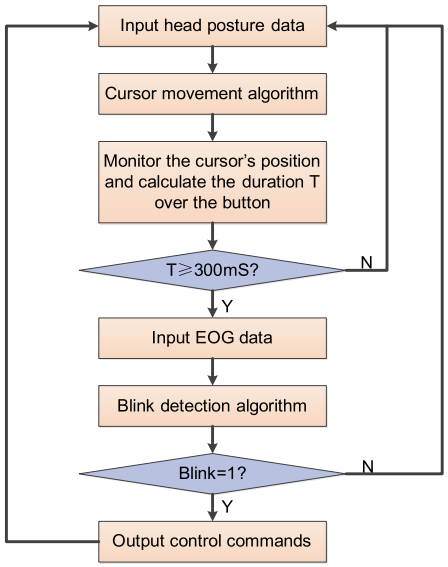

Fig. 7. Decision making flow.

3) Decision Making: The decision-making process of the BCI system, as illustrated in Fig. 7, involves several steps. First, the cursor movement algorithm translates the head posture into the cursor position. Second, the system monitors the cursor position, calculates the duration T_b it remains over a button, and checks whether T_b exceeds 300 ms. If T_b exceeds 300 ms, a blinking detection algorithm is performed to check whether a valid blink exists. Finally, if a valid blink exists, the system issues the command of the corresponding button.

F. Calibration

Due to the variations in EOG signals among individuals, it's essential to calibrate the EOG template individually for blinking detection. EOG data of 10 blinks with a 2-s interval between consecutive blinks were collected after the system's animation and voice prompts, and we extracted a 2-s segment with 500 sampling points after the prompts. After baseline correction and bandpass filtering of these 10 segments, we symmetrically choose 74 data points around the peak of each, creating 10 new segments, each comprising 149 data points. A weighted average of these new segments yields the template EOG waveform. The blinking detection threshold is set as described in the Blinking Detection, and the system updates the thresholds automatically.

G. Performance Metrics

The performance metrics of the system are listed and introduced in TABLE I. Task time (TT), accuracy (Acc), response time (RT), information transfer rate (ITR), false trigger rate (FTR), and stop response time (SRT) were recorded in the experiment. Specifically, the ITR is a metric used to evaluate the efficiency of BCI systems in processing information, which records the bits of information transferred per minute. It is defined by [48]:

$$\mathrm{ITR} = 60\left(\log_2 M + P\log_2 P + (1-P)\log_2\left(\frac{1-P}{M-1}\right)\right)/T \tag{11}$$

TABLE I
PERFORMANCE METRICS OF THE SYSTEM

Performance Metrics	Description
Task time (TT)	Time required to complete the task in the experiment
Accuracy (Acc)	Ratio of the number of correctly executed commands to the number of commands issued in the experimental task
Response time (RT)	Time required to issue a command
Information transfer rate (ITR)	Bits of information transferred per minute
False trigger rate (FTR)	Number of false triggered commands per minute during the idle time
Stop response time (SRT)	Time required to issue a stop command for the electric nursing bed

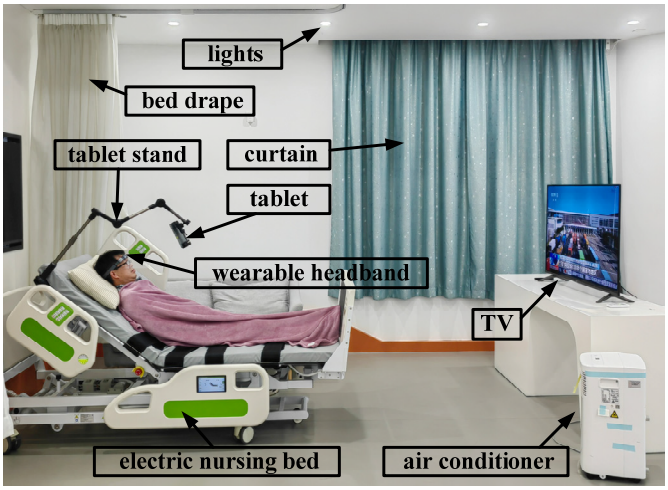

Fig. 8. Experimental scene of the smart ward.

where M is the number of command types, P is the average accuracy, and T is the average RT recorded in minute. Due to the varying number of buttons in different GUI within the proposed system, the ITR is recorded as a range.

Furthermore, we evaluated the workload of the users when they were performing the experimental tasks. NASA-TLX was used to evaluate the level of workload experienced by users while interacting with the proposed BCI system. It consists of 6 subscales: mental demand, physical demand, temporal demand, performance, effort, and frustration [49], [50]. Each subscale is scored on a 100-point scale. Users assess each of the subscale and score according to their experienced workload.

Based on the scoring criteria of the NASA-TLX scale, higher scores denote a higher workload, whereas lower scores suggest a lighter workload. In this study, users filled out the NASA-TLX questionnaire after the experimental tasks.

III. EXPERIMENTS AND RESULTS

A. Experiment I: Smart Ward Control

To evaluate the performance of the system, 10 participants performed designed tasks simulating the daily activities of patients with extremity motor function issues. During the experiment, participants wore the headband, lay down on the electric nursing bed, and adjusted the tablet computer's

position to have a clear view. All participants were provided with a comprehensive overview of the system and the experimental task which included instructions on cursor control and smart ward operation. They carried out some control operations themselves and adjusted some scaling factors to better control the cursor. When the participants were clear about the control method, we started the smart ward control task. During the task, the system displayed a to-do prompt above the screen. If an incorrect click occurs, the system logged the error and indicated it with a red flashing prompt, showed the correct instruction, and guided the participants to correct the mistake. The experimental scene of the smart ward is shown in Fig. 8.

First, participants performed a short EOG calibration for blinking detection, in which they performed 10 eye blinks in accordance with the system prompt, taking approximately 20 s. Subsequently, each of them completed two tasks, which included a smart ward control task and a one-hour idle state task. In terms of the smart ward control task, 43 commands (Cmds) were issued in the following order.

1) Unlock the system to enter the smart ward GUI (1 Cmd); 2) Switch to the lighting control GUI, turn on the lights (2 Cmds); 3) Switch to the bed drape control GUI, open the bed drape (2 Cmds); 4) Switch to the air conditioning control GUI, turn on the air conditioner, switch to cooling mode, increase the set temperature by 1°C, and set the wind speed to medium (5 Cmds); 5) Switch to the electric nursing bed control GUI and perform the following actions in sequence: Raise legs (for 10 s), raise back (for 10 s), raise back and legs simultaneously (for 10 s), raise the bed (for 10 s) (5 Cmds); 6) Switch to the TV control GUI, Turn on the TV, navigate to the TV main menu page, press the down arrow key once, press the right arrow key twice, press the down arrow key once, press the left arrow key once, press the up arrow key once, press the OK key, decrease the volume by 2 units, increase the volume by 1 unit, lock the system, watch for 5 minutes, unlock the system, and turn off the TV (16 Cmds); 7) Switch to the electric nursing bed control GUI and perform the following actions in sequence: Lower legs (for 10 s), lower back (for 10 s), lower back and legs simultaneously (for 10 s), lower the bed (for 10 s) (5 Cmds); 8) Switch to the air conditioning control GUI and turn off the air conditioning (2 Cmds); 9) Switch to the curtain control GUI, close the curtain (2 Cmds); 10) Switch to the lighting control GUI, turn off the lights (2 Cmds); 11) Lock the system (1 Cmd). During the task, TT, Acc, and RT were recorded, and ITR was calculated. The TT excluded the running time of the smart ward equipment.

When finishing the smart ward control task, the participants first performed tasks in Experiment II (mentioned in Section III-B). Afterwards, the participants performed a one-hour idle state task to evaluate the stability of the proposed system during an extended idle state. The system was set to a locked state, and participants were free to do routine activities such as blinking, turning head, talking, browsing the internet, resting, and so on. During the task, FTR was recorded.

In Experiment I, all 10 participants successfully accomplished the smart ward control task, and the results are listed in TABLE II. With an average task time of 76.9 s, the average accuracy reached 97.0 ± 3.9 %, with nine participants exceeding 90%, and five making no mistake. In terms of the average response time, 2.39 ± 0.53 s was achieved. Through calculation, the average ITR reached 97.6 ± 29.7 bits/min. In the idle state task, no false trigger was activated by any participant, so the FTR was recorded as 0 event per minute.

TABLE II
RESULTS OF SMART WARD CONTROL EXPERIMENT

Participant	TT (s)	Acc (%)	RT (s)	ITR (bit/min)
P1	77.7	100	2.35	100.7 (91.5-112.1)
P2	66.8	89.1	2.23	81.5 (72.9-92.1)
P3	64.3	97.3	2.01	109.3 (98.9-122.3)
P4	71.7	100	2.04	116.0 (105.4-129.2)
P5	65.5	91.9	2.18	88.8 (79.8-100.1)
P6	87.7	100	2.65	89.3 (81.2-99.4)
P7	93.7	97.3	2.92	75.3 (68.1-84.2)
P8	92.9	94.6	2.99	68.9 (62.1-77.4)
P9	45.9	100	1.39	170.3 (154.8-189.6)
P10	102.7	100	3.11	76.1 (69.2-84.7)
Avg.±SD	76.9±17.3	97.0±3.9	2.39±0.53	97.6±29.7

B. Experiment II: Electric Nursing Bed Control

After the smart ward control task in Experiment I, 10 participants performed designed tasks simulating the daily control of electric nursing bed of patients with extremity motor function issues, to independently evaluate the performance of electric nursing bed control. Note that the electric nursing bed achieved continuous control rather than step control with preset operation steps. The experimental procedure is similar to that in Experiment I. Each of the participant completed two tasks, which included an electric nursing bed control task and an electric nursing bed stop task. In terms of the electric nursing bed control task, and the command procedure is as follows.

1) Unlock the system to enter the control interface for the electric nursing bed, which contains 9 control buttons (8 for the bed control and 1 for locking the system); 2) Raise the electric nursing bed from the lowest position to the highest position; 3) Perform the first posture adjustment by pressing the elevation buttons for the backrest and leg rest in turn, transforming the user from a lying flat position to a sitting position; 4) Press the lowering buttons for the backrest and leg rest in turn to return the user to a lying flat position. 5) Perform the second posture adjustment by pressing the simultaneous elevation button for both the backrest and leg rest to adjust the user from a lying flat position to a sitting position again; 6) press the simultaneous lowering button for both the backrest and leg rest to let the user lie flat once more; 7) lower the electric nursing bed from the highest position to the lowest position; 8) Lock the system. During the task, Acc and TT were recorded. Since the electric nursing bed achieved continuous control, the TT included the running time of the electric nursing bed.

When finishing the electric nursing bed control task, the participants performed an electric nursing bed stop task. In this task, participants were free to operate the electric nursing

TABLE III
RESULT OF ELECTRIC NURSING BED CONTROL EXPERIMENT

Participant	Control TT (s)		Stop Task SRT (s)	
	Manual Control	BCI Control	Manual Control	BCI Control
P1	268	266	0.71	0.82
P2	253	271	0.65	0.70
P3	258	283	0.58	0.69
P4	252	278	0.53	0.60
P5	251	273	0.75	0.87
P6	253	288	0.65	0.75
P7	250	282	0.69	0.80
P8	262	281	0.53	0.57
P9	255	289	0.63	0.69
P10	260	275	0.67	0.82
Avg.±SD	256.2±5.7	278.6±7.4	0.64±0.07	0.73±0.10

bed, and the system randomly issued stop command 40 times. Participants stopped the bed's movement as soon as possible after the prompt. During the task, Acc and SRT were recorded.

A manual control session of the two tasks was also performed together with the BCI control session. All the control order in the manual control session was identical to that of the BCI control session. All participants performed the two sessions in a random order.

In Experiment II, all 10 participants successfully accomplished the electric nursing bed control and stop tasks, and the results are listed in TABLE III. During the electric nursing bed control task, all participants achieved an accuracy of 100% in both the BCI and the manual control sessions. In terms of the control task time, 278.6 ± 7.4 s and 256.2 ± 5.7 s ($p < 0.001$, paired t-test) were achieved in the BCI and the manual control session respectively. Note that the control task time includes a fixed 241 s of electric nursing bed running time. During the electric nursing bed stop task, all participants also achieved an accuracy of 100% in both the BCI and the manual control sessions. In terms of the stop response time, 0.64 ± 0.07 s and 0.73 ± 0.10 s ($p < 0.001$, paired t-test) were achieved in the BCI and the manual control session respectively. Although significant differences were observed in both task time and stop response time between the two methods, the absolute time differences are relatively small and fully acceptable for practical applications.

In addition, we further analyzed the β/θ ratio of the 10 participants in both attentive (voluntary blinks) and inattentive (involuntary blinks) states, as illustrated in Fig. 9. With all participants showing a higher β/θ ratio in the attentive state than in the inattentive state, statistical analysis (independent t-test) revealed that 9 out of the 10 participants exhibited a significant difference between the two states. These results indicate that the system effectively distinguished voluntary and involuntary blinking.

C. Workload Evaluation

After completing the experiment, each participant performed a workload evaluation based on NASA-TLX according

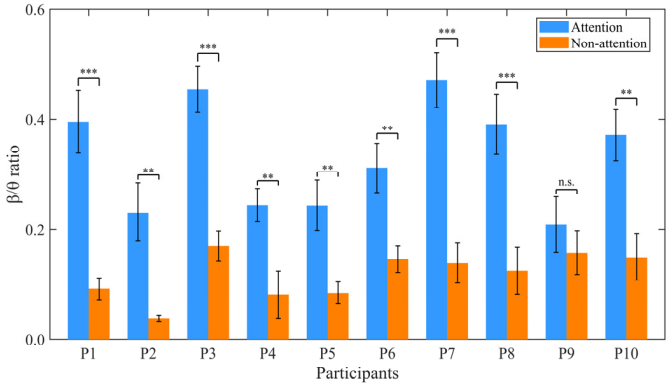

Fig. 9. Results of the β/θ ratio of the 10 participants in both attentive (voluntary blinks) and inattentive (involuntary blinks) states. The "n.s.", "*", "**", "***" indicate the significance level of the paired-sample T-test between the experiment and control sessions, with $p \geq 0.05$, $p \geq 0.05$, $p < 0.01$, and $p < 0.001$, respectively.

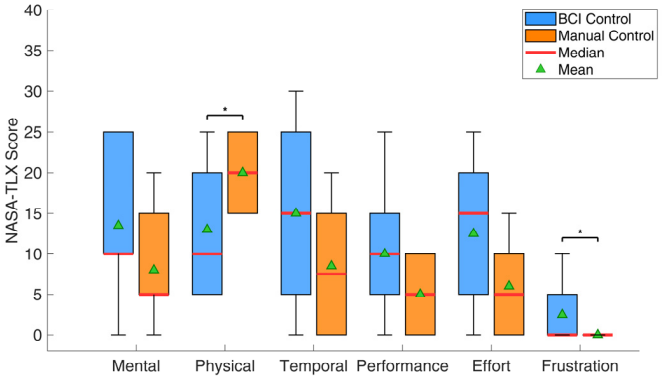

Fig. 10. Results of NASA-TLX-based workload evaluation for 10 participants using BCI control and manual control methods. The "*", "***", "****" indicate the significance level of the paired-sample T-test between the experiment and control sessions, with $p \geq 0.05$, $p < 0.01$, and $p < 0.001$, respectively.

to their perceived workload when using the system. The perceived workload using BCI control and manual control methods was given by each participant respectively, and the result of the workload evaluation is visualized in Fig. 10. When using the BCI control method, the average scores of mental demand, physical demand, temporal demand, performance, effort, and frustration were 13.5 ± 8.8, 13.0 ± 7.9, 15.0 ± 10.0, 10.0 ± 7.1, 12.5 ± 8.6, and 2.5 ± 3.5. When using the manual control method, all 6 average scores were 8.0 ± 6.8, 17.7 ± 3.7, 8.5 ± 7.5, 5.0 ± 4.1, 6.0 ± 5.2, and 0.3 ± 0.5.

Furthermore, a paired t-test was conducted to analyze the workload differences between the two control methods. In the physical demand dimension, the BCI method had a significantly lower average score than the manual control method ($p < 0.05$), indicating a lower physical workload for BCI control. In the frustration dimension, the BCI method showed a significantly lower average score compared to the manual control method ($p < 0.05$), indicating less frustration for manual control. No significant differences were found between the two control methods in the remaining 4 dimensions namely

TABLE IV
PERFORMANCE COMPARISON WITH OTHER METHODS

Reference	Signals	Command Number	Control Target	Acc (%)	ITR (bits/min)	FTR (event/min)	Health Status
Zhang et al **[51]**	EOG	16	5	93.6	26.8	0.1	Patient
Molleapaza-Huanaco et al **[52]**	EOG	4	5	**97.71**	49.19	—	Healthy
Ghaffar et al **[53]**	IMU+EOG	19	4	81.48	—	—	Healthy
Chai et al **[54]**	SSVEP+EMG	9	6	83.6	45	—	Patient
Zhu et al **[55]**	EOG+SSVEP	15	1	92.09	35.98	—	Healthy
Shukla et al **[56]**	P300	6	6	89.33	—	0.162	Patient
Tonin et al **[57]**	MI	2	1	81.4	11.26	—	Patient
Li et al **[19]**	EOG+MI+SSVEP	8	1	96.7	—	—	Healthy
Our system	IMU+EOG+EEG	**20**	**6**	97.0	**97.6**	**0**	Healthy

mental demand, temporal demand, performance and effort ($p \geq 0.05$).

Overall, the average scores of all 6 subscales using both control methods were lower than 20 points, suggesting the participants experienced a relatively low overall workload when using our proposed system.

IV. DISCUSSION

In this paper, we developed a wearable BCI system for smart ward control. By wearing a wireless headband, participants were able to control a smart ward with head rotation and eye blinking. To our satisfaction, all participants fully completed the tasks, and the results demonstrated the effectiveness of the system. In this section, we discuss the system performance and experimental results. We analyze the experimental results and our system performance with that of previous high-performing systems. Furthermore, we address some limitations of this work and outline future research directions.

Overall, our system shows satisfactory performance in key performance metrics. First, by integrating gyroscope and EOG signals, the output command set is expanded, meeting the need for more complex control. The system can provide over 20 control commands, with 6 control targets, the highest among all systems listed in the table. It can be further expanded according to practical need. Second, the blinking detection algorithm, combining similarity and energy, effectively improves the system's control accuracy without compromising the ITR. The accuracy of our system reaches 97.0%, and the ITR climbs to 97.6 bits/min. Moreover, the system can effectively distinguish between working and idle states, achieving a very low FPR, which enhances its practicality. Finally, the proposed system is a lightweight wearable BCI system, providing a comfortable user experience when the user is lying down. The dry electrodes are made from soft hydrogel material, which easily conforms to the skin and is deformable on the surface. The elastic fabric structure allows users to easily adjust the tightness, greatly improving the user experience and laying a solid foundation for clinical translation and daily assistive applications.

These design features lay a solid foundation for the system's practicality, and to further verify its applicability in real assistive scenarios, we compared its performance and workload with traditional manual control. Results show both the BCI system and manual control achieve 100% accuracy in nursing bed control and stop tasks, ensuring reliable basic operation. The BCI system has some performance differences, such as slightly longer task time, but given that it does not rely on peripheral nerves, this performance is already impressive for a BCI system. From workload feedback, participants reported that manual control imposes higher physical demand. This is because manual control requires constant hand-raising, and participants noted that this leads to hand fatigue. The minor differences in frustration between the two methods come from gaps in control efficiency. This is because manual control is more efficient due to direct hand operation while the BCI system has slight delays. Additionally, the two methods show no differences in mental demand, temporal demand, performance, or effort, which indicates the BCI system does not add extra cognitive or time burdens for users. Overall, the differences between the two methods are fully acceptable, and the BCI system's average workload across all dimensions is below 20 points, which further confirms its favorable user acceptance. Notably, this study only conducted a single experimental session for each participant. However, the low workload with an average score below 20 and the simple calibration process which only takes about 20 s for eye-blink calibration and involves no redundant learning steps suggest the system is suitable for long-term use. It is reasonable to anticipate that participants would become more proficient with repeated use, which would further improve the system's practicality by enhancing their performance including reduced task time and more stable operation. For assistive living scenarios, the BCI system's feature of not relying on extremities is particularly important, making it a practical solution for users with limited extremities function.

Beyond validating against manual control, we compare the performance of our proposed BCI system with that of previous high-performing HCI systems as shown in TABLE IV. The core advantage of this study lies in the integration of its highly wearable EEG acquisition system (a lightweight headband) with a real-world smart ward environment. Compared to the traditional EEG caps widely used in existing research (e.g., the devices relying on wet electrodes and complex wiring in [19], [51], [54], [55], [56], [57], and [58]), our headband design

significantly enhances user comfort and feasibility for long-term use. For instance, while the EOG system by Zhang et al. achieved 93.6% accuracy in smart home control, its reliance on wet electrodes limited its practical application scenarios [51]. Similarly, the hybrid BCI systems by Chai et al. [54] and the SSVEP/EOG system by Zhu et al. required multi-channel EEG caps [55], making them unsuitable for dynamic daily environments. In contrast, our system achieves high-precision signal acquisition in a real smart ward through a lightweight headband, avoiding the bulkiness and operational complexity of traditional EEG caps, thus providing a critical foundation for clinical translation.

In terms of performance metrics, our system achieves 97.0% accuracy and an ITR of 93.8–107 bits/min, significantly outperforming most literature-reported schemes. For example, a traditional EOG human-machine system by Molleapaza-Huanaco et al. reached 97.71% accuracy but had an ITR of only 49.19 bits/min [52]. The ITR of the P300 asynchronous system was relatively low, at 11.19 bits/min [56]. Even hybrid systems, such as the SSVEP/EOG system by Zhu et al. which achieved 92.09% accuracy and 35.98 bits/min ITR [55] and the SSVEP/EMG system by Chai et al. which had 83.6% accuracy and 45 bits/min ITR in the patient group [54], were limited in performance by the complexity of multimodal signal fusion. These systems often prioritize accuracy over response speed. Our proposed BCI system stands out with 97.0% accuracy and an ITR ranging from 93.8 to 107 bits/min, successfully balancing both accuracy and response speed.

The FTR during the idle state is a critical safety metric for medical BCI systems. Our system achieves a zero FTR, which is realized through the integration and co-judgment of multimodal signals to enable reliable asynchronous control. This design is particularly crucial for severely impaired patients; for instance, in nursing bed control, false triggers could pose risks such as unintended postural changes, and our zero-FTR feature effectively ensures clinical safety. For reference, some systems reported in existing literature have different performance in this aspect: the P300 system by Shukla et al. had a FTR of 0.15–0.162 events/min in asynchronous mode [56], while the EOG system by Zhang et al. had a FTR of 0.1 events/min [51]. These reported systems have already achieved considerable performance in reducing false triggers, and our system further elevates this capability by realizing a zero FTR, which underscores the enhanced reliability of our design for clinical applications.

Although the BCI system proposed in this study demonstrates significant practicality and application potential, it still has certain limitations. First, this study only conducted a single experimental session, so the learning effect of participants which refers to how their performance improves with repeated use was not fully explored. Second, the study primarily focuses on healthy participant, leaving the applicability to patients uncertain. Future works should involve implementation of the system to individuals with motor impairments. Moreover, analyzing user behaviors and habits to optimize control strategies and achieve more personalized interaction experiences can enhance the system's practicality. Furthermore, for patients with limited head mobility, the integration of EEG and EMG signals may enable more precise and natural interaction, and enhance both user experience and acceptance, thereby providing greater convenience and support to those in need. Additionally, the current blink detection mechanism does not account for situations such as multiple consecutive blinks, and future studies will integrate supplementary deciding mechanisms to address this issue and enhance detection robustness.

V. Conclusion

In this study, we proposed a wearable multimodal BCI system for smart ward control, which employs a self-designed wearable headband to capture EOG signals and head posture. By wearing the headband, users can control a computer cursor on the screen only with head rotation and eye blinking, and further control devices in a smart ward with self-designed GUIs. The system decodes gyroscope data to map the head posture to the position of the cursor on the screen and decodes EOG signals to detect valid blinks for selecting and activating function buttons. 10 participants were recruited to perform two experimental tasks that simulate the daily needs of patients with extremity motor function issues. To our satisfaction, all the participants fully accomplished the simulated tasks, and an average accuracy of 97.0 ± 3.9 % and an average response time of 2.39 ± 0.53 s were achieved. Different from traditional step-controlled BCI nursing beds, we designed a continuous-controlled nursing bed and achieved satisfactory results. Furthermore, workload evaluation using NASA-TLX revealed that the participants experienced a low workload when using the system. The experimental results demonstrate the effectiveness of our proposed system, indicating significant potential for practical applications.

References

[1] P.-A. Albinsson and S. Zhai, "High precision touch screen interaction," in *Proc. SIGCHI Conf. Hum. Factors Comput. Syst.*, Apr. 2003, pp. 105–112, doi: 10.1145/642611.642631.

[2] Y. Song, D. Demirdjian, and R. Davis, "Continuous body and hand gesture recognition for natural human-computer interaction," *ACM Trans. Interact. Intell. Syst.*, vol. 2, no. 1, pp. 1–28, Mar. 2012, doi: 10.1145/2133366.2133371.

[3] J. Goulding, W. Nadim, P. Petridis, and M. Alshawi, "Construction industry offsite production: A virtual reality interactive training environment prototype," *Adv. Eng. Informat.*, vol. 26, no. 1, pp. 103–116, Jan. 2012, doi: 10.1016/j.aei.2011.09.004.

[4] F. Zhou, H. B.-L. Duh, and M. Billinghurst, "Trends in augmented reality tracking, interaction and display: A review of ten years of ISMAR," in *Proc. 7th IEEE/ACM Int. Symp. Mixed Augmented Reality*, Sep. 2008, pp. 193–202, doi: 10.1109/ISMAR.2008.4637362.

[5] R. Amalberti, N. Carbonell, and P. Falzon, "User representations of computer systems in human-computer speech interaction," *Int. J. Man-Mach. Stud.*, vol. 38, no. 4, pp. 547–566, Apr. 1993, doi: 10.1006/imms.1993.1026.

[6] M. C. Kiernan et al., "Improving clinical trial outcomes in amyotrophic lateral sclerosis," *Nature Rev. Neurol.*, vol. 17, no. 2, pp. 104–118, Feb. 2021, doi: 10.1038/s41582-020-00434-z.

[7] N. S. Card et al., "An accurate and rapidly calibrating speech neuroprosthesis," *New England J. Med.*, vol. 391, no. 7, pp. 609–618, Aug. 2024, doi: 10.1056/nejmoa2314132.

[8] K. Li, D. Chen, Z. Rao, Z. Guan, Y. Jiang, and Y. Li, "A multimodal asynchronous human-machine interaction method based on electrooculography and speech recognition for wheelchair control," *IEEE Sensors J.*, vol. 24, no. 23, pp. 39195–39205, Dec. 2024, doi: 10.1109/JSEN.2024.3432076.

[9] L. Rundo, R. Pirrone, S. Vitabile, E. Sala, and O. Gambino, "Recent advances of HCI in decision-making tasks for optimized clinical workflows and precision medicine," *J. Biomed. Informat.*, vol. 108, Aug. 2020, Art. no. 103479, doi: 10.1016/j.jbi.2020.103479.

[10] R. Zhang et al., "Control of a wheelchair in an indoor environment based on a brain–computer interface and automated navigation," *IEEE Trans. Neural Syst. Rehabil. Eng.*, vol. 24, no. 1, pp. 128–139, Jan. 2016, doi: 10.1109/TNSRE.2015.2439298.

[11] Y. Zhou et al., "Shared three-dimensional robotic arm control based on asynchronous BCI and computer vision," *IEEE Trans. Neural Syst. Rehabil. Eng.*, vol. 31, pp. 3163–3175, 2023, doi: 10.1109/TNSRE.2023.3299350.

[12] B. Liu, Y. Wang, X. Gao, and X. Chen, "EldBETA: A large eldercare-oriented benchmark database of SSVEP-BCI for the aging population," *Sci. Data*, vol. 9, no. 1, p. 252, May 2022, doi: 10.1038/s41597-022-01372-9.

[13] W. Wei, Q. Dai, Y. Wong, Y. Hu, M. Kankanhalli, and W. Geng, "Surface-electromyography-based gesture recognition by multi-view deep learning," *IEEE Trans. Biomed. Eng.*, vol. 66, no. 10, pp. 2964–2973, Oct. 2019, doi: 10.1109/TBME.2019.2899222.

[14] R. Barea, L. Boquete, M. Mazo, and E. Lopez, "System for assisted mobility using eye movements based on electrooculography," *IEEE Trans. Neural Syst. Rehabil. Eng.*, vol. 10, no. 4, pp. 209–218, Dec. 2002, doi: 10.1109/TNSRE.2002.806829.

[15] Z. Lu et al., "A wearable human–machine interactive instrument for controlling a wheelchair robotic arm system," *IEEE Trans. Instrum. Meas.*, vol. 73, pp. 1–15, 2024, doi: 10.1109/TIM.2024.3376685.

[16] R. Zhang et al., "A BCI-based environmental control system for patients with severe spinal cord injuries," *IEEE Trans. Biomed. Eng.*, vol. 64, no. 8, pp. 1959–1971, Aug. 2017, doi: 10.1109/TBME.2016.2628861.

[17] Y. Jiang, K. Li, Y. Liang, D. Chen, M. Tan, and Y. Li, "Daily assistance for amyotrophic lateral sclerosis patients based on a wearable multimodal brain-computer interface mouse," *IEEE Trans. Neural Syst. Rehabil. Eng.*, vol. 33, pp. 150–161, 2025, doi: 10.1109/TNSRE.2024.3520984.

[18] C.-T. Lin, B.-S. Lin, F.-C. Lin, and C.-J. Chang, "Brain computer interface-based smart living environmental auto-adjustment control system in UPnP home networking," *IEEE Syst. J.*, vol. 8, no. 2, pp. 363–370, Jun. 2014, doi: 10.1109/JSYST.2012.2192756.

[19] Y. Li, T. Zheng, M. Wang, L. Dong, P. Wang, and X. Qin, "A coloring and timing brain-computer interface for the nursing bed robot," *Comput. Electr. Eng.*, vol. 95, Oct. 2021, Art. no. 107415, doi: 10.1016/j.compeleceng.2021.107415.

[20] E. Pasqualotto, S. Federici, and M. O. Belardinelli, "Toward functioning and usable brain–computer interfaces (BCIs): A literature review," *Disab. Rehabil., Assistive Technol.*, vol. 7, no. 2, pp. 89–103, Mar. 2012, doi: 10.3109/17483107.2011.589486.

[21] G. Liberati et al., "Developing brain-computer interfaces from a user-centered perspective: Assessing the needs of persons with amyotrophic lateral sclerosis, caregivers, and professionals," *Appl. Ergonom.*, vol. 50, pp. 139–146, Sep. 2015, doi: 10.1016/j.apergo.2015.03.012.

[22] Z. Rao et al., "A once-calibration brain-computer interface to enhance convenience for continuous BCI interventions in stroke patients," *IEEE Sensors J.*, vol. 25, no. 2, pp. 3949–3963, Jan. 2025, doi: 10.1109/JSEN.2024.3510059.

[23] W. Gao et al., "Learning invariant patterns based on a convolutional neural network and big electroencephalography data for subject-independent P300 brain-computer interfaces," *IEEE Trans. Neural Syst. Rehabil. Eng.*, vol. 29, pp. 1047–1057, 2021, doi: 10.1109/TNSRE.2021.3083548.

[24] J. E. Huggins, A. A. Moinuddin, A. E. Chiodo, and P. A. Wren, "What would brain-computer interface users want: Opinions and priorities of potential users with spinal cord injury," *Arch. Phys. Med. Rehabil.*, vol. 96, no. 3, pp. S38–S45.e5, Mar. 2015, doi: 10.1016/j.apmr.2014.05.028.

[25] J. P. Donoghue, "Bridging the brain to the world: A perspective on neural interface systems," *Neuron*, vol. 60, no. 3, pp. 511–521, Nov. 2008, doi: 10.1016/j.neuron.2008.10.037.

[26] N. Birbaumer and L. G. Cohen, "Brain–computer interfaces: Communication and restoration of movement in paralysis," *J. Physiol.*, vol. 579, no. 3, pp. 621–636, Mar. 2007, doi: 10.1113/jphysiol.2006.125633.

[27] M. Kopecek and J. Kremlacek, "Eye-tracking control of an adjustable electric bed: Construction and validation by immobile patients with multiple sclerosis," *J. NeuroEng. Rehabil.*, vol. 20, no. 1, p. 75, Jun. 2023, doi: 10.1186/s12984-023-01193-w.

[28] Y. Dong and F. Duan, "The design of a nursing bed based on eye movement control," in *Proc. 42nd Chin. Control Conf. (CCC)*, Jul. 2023, pp. 4083–4088, doi: 10.23919/CCC58697.2023.10240523.

[29] A. F. Klaib, N. O. Alsrehin, W. Y. Melhem, H. O. Bashtawi, and A. A. Magableh, "Eye tracking algorithms, techniques, tools, and applications with an emphasis on machine learning and Internet of Things technologies," *Expert Syst. Appl.*, vol. 166, Mar. 2021, Art. no. 114037, doi: 10.1016/j.eswa.2020.114037.

[30] J. Li, J. Zhu, and C. Guan, "Assessing illumination fatigue in tunnel workers through eye-tracking technology: A laboratory study," *Adv. Eng. Informat.*, vol. 59, Jan. 2024, Art. no. 102335, doi: 10.1016/j.aei.2023.102335.

[31] S. He and Y. Li, "A single-channel EOG-based speller," *IEEE Trans. Neural Syst. Rehabil. Eng.*, vol. 25, no. 11, pp. 1978–1987, Nov. 2017, doi: 10.1109/TNSRE.2017.2716109.

[32] Q. Huang et al., "An EOG-based human–machine interface for wheelchair control," *IEEE Trans. Biomed. Eng.*, vol. 65, no. 9, pp. 2023–2032, Sep. 2018, doi: 10.1109/TBME.2017.2732479.

[33] N.-H. Liu, C.-Y. Chiang, and H.-C. Chu, "Recognizing the degree of human attention using EEG signals from mobile sensors," *Sensors*, vol. 13, no. 8, pp. 10273–10286, Aug. 2013, doi: 10.3390/s130810273.

[34] L. Hu, J. Zhu, S. Chen, Y. Zhou, Z. Song, and Y. Li, "A wearable asynchronous brain-computer interface based on EEG-EOG signals with fewer channels," *IEEE Trans. Biomed. Eng.*, vol. 71, no. 2, pp. 504–513, Feb. 2024, doi: 10.1109/TBME.2023.3308371.

[35] Z. Rao et al., "A wearable brain-computer interface with fewer EEG channels for online motor imagery detection," *IEEE Trans. Neural Syst. Rehabil. Eng.*, vol. 32, pp. 4143–4154, 2024, doi: 10.1109/TNSRE.2024.3502135.

[36] A. Angelidis, W. van der Does, L. Schakel, and P. Putman, "Frontal EEG theta/beta ratio as an electrophysiological marker for attentional control and its test-retest reliability," *Biol. Psychol.*, vol. 121, pp. 49–52, Dec. 2016, doi: 10.1016/j.biopsycho.2016.09.008.

[37] P. Putman, B. Verkuil, E. Arias-Garcia, I. Pantazi, and C. van Schie, "EEG theta/beta ratio as a potential biomarker for attentional control and resilience against deleterious effects of stress on attention," *Cognit., Affect., Behav. Neurosci.*, vol. 14, no. 2, pp. 782–791, Jun. 2014, doi: 10.3758/s13415-013-0238-7.

[38] H. N. Isiten, M. Cebi, B. Sutcubasi Kaya, B. Metin, and N. Tarhan, "Medication effects on EEG biomarkers in attention-deficit/hyperactivity disorder," *Clin. EEG Neurosci.*, vol. 48, no. 4, pp. 246–250, Jul. 2017, doi: 10.1177/1550059416675232.

[39] W. Klimesch, M. Doppelmayr, H. Russegger, T. Pachinger, and J. Schwaiger, "Induced alpha band power changes in the human EEG and attention," *Neurosci. Lett.*, vol. 244, no. 2, pp. 73–76, Mar. 1998, doi: 10.1016/s0304-3940(98)00122-0.

[40] H. Huang et al., "Real-time attention regulation and cognitive monitoring using a wearable EEG-based BCI," *IEEE Trans. Biomed. Eng.*, vol. 72, no. 2, pp. 716–724, Feb. 2025, doi: 10.1109/TBME.2024.3468351.

[41] J. Mercado, L. Escobedo, and M. Tentori, "A BCI video game using neurofeedback improves the attention of children with autism," *J. Multimodal User Interface*, vol. 15, no. 3, pp. 273–281, Sep. 2021, doi: 10.1007/s12193-020-00339-7.

[42] W. Huang, W. Wu, M. V. Lucas, H. Huang, Z. Wen, and Y. Li, "Neurofeedback training with an electroencephalogram-based brain-computer interface enhances emotion regulation," *IEEE Trans. Affect. Comput.*, vol. 14, no. 2, pp. 998–1011, Apr. 2023, doi: 10.1109/TAFFC.2021.3134183.

[43] H. Huang et al., "An EEG-based brain computer interface for emotion recognition and its application in patients with disorder of consciousness," *IEEE Trans. Affect. Comput.*, vol. 12, no. 4, pp. 832–842, Oct. 2021, doi: 10.1109/TAFFC.2019.2901456.

[44] K. Li et al., "An electroencephalography-based brain–computer interface for emotion regulation with virtual reality neurofeedback," *IEEE Trans. Cognit. Develop. Syst.*, vol. 16, no. 4, pp. 1405–1417, Aug. 2024, doi: 10.1109/TCDS.2024.3357547.

[45] L. J. Trejo, K. Kubitz, R. Rosipal, R. L. Kochavi, and L. D. Montgomery, "EEG-based estimation and classification of mental fatigue," *Psychology*, vol. 6, no. 5, pp. 572–589, 2015, doi: 10.4236/psych.2015.65055.

[46] E. Wascher et al., "Frontal theta activity reflects distinct aspects of mental fatigue," *Biol. Psychol.*, vol. 96, pp. 57–65, Feb. 2014, doi: 10.1016/j.biopsycho.2013.11.010.

[47] A. R. Clarke, R. J. Barry, R. McCarthy, M. Selikowitz, D. C. Clarke, and R. J. Croft, "Effects of stimulant medications on children with attention-deficit/hyperactivity disorder and excessive beta activity in their EEG," *Clin. Neurophysiol.*, vol. 114, no. 9, pp. 1729–1737, Sep. 2003, doi: 10.1016/s1388-2457(03)00112-3.

[48] Y. Yu, Y. Liu, E. Yin, J. Jiang, Z. Zhou, and D. Hu, "An asynchronous hybrid spelling approach based on EEG–EOG signals for Chinese character input," *IEEE Trans. Neural Syst. Rehabil. Eng.*, vol. 27, no. 6, pp. 1292–1302, Jun. 2019, doi: 10.1109/TNSRE.2019.2914916.

[49] S. G. Hart and M. Field, "NASA-task load Index (NASA-TLX); 20 Years later," in *Proc. Hum. Factors Ergonom. Soc. Annu. Meeting*, vol. 50, no. 9. Los Angeles, CA, USA: Sage Publications, Oct. 2006, pp. 904–908, doi: 10.1177/154193120605000909.

[50] J. M. Noyes and D. P. J. Bruneau, "A self-analysis of the NASA-TLX workload measure," *Ergonomics*, vol. 50, no. 4, pp. 514–519, Apr. 2007, doi: 10.1080/00140130701235232.

[51] R. Zhang et al., "An EOG-based human–machine interface to control a smart home environment for patients with severe spinal cord injuries," *IEEE Trans. Biomed. Eng.*, vol. 66, no. 1, pp. 89–100, Jan. 2019, doi: 10.1109/TBME.2018.2834555.

[52] J. Molleapaza-Huanaco, H. Charca-Morocco, B. Juarez-Chavez, R. Equino-Quispe, J. Talavera-Suarez, and E. Mayhua-Lopez, "IoT platform based on EOG to monitor and control a smart home environment for patients with motor disabilities," in *Proc. 13th Int. Congr. Image Signal Process., Biomed. Eng. Informat. (CISP-BMEI)*, Morocco. China, Oct. 2020, pp. 784–789, doi: 10.1109/CISP-BMEI51763.2020.9263534.

[53] M. Ghaffar, S. R. Sheikh, N. Naseer, and F. Ahmed, "Assistive smart home environment using head gestures and EEG eye blink control schemes," in *IEEE MTT-S Int. Microw. Symp. Dig.*, Apr. 2021, pp. 1–6, doi: 10.1109/AIMS52415.2021.9466031.

[54] X. Chai et al., "A hybrid BCI-controlled smart home system combining SSVEP and EMG for individuals with paralysis," *Biomed. Signal Process. Control*, vol. 56, Feb. 2020, Art. no. 101687, doi: 10.1016/j.bspc.2019.101687.

[55] Y. Zhu, Y. Li, J. Lu, and P. Li, "A hybrid BCI based on SSVEP and EOG for robotic arm control," *Frontiers Neurorobotics*, vol. 14, Nov. 2020, Art. no. 583641, doi: 10.3389/fnbot.2020.583641.

[56] P. K. Shukla, R. K. Chaurasiya, S. Verma, and G. R. Sinha, "A thresholding-free state detection approach for home appliance control using P300-based BCI," *IEEE Sensors J.*, vol. 21, no. 15, pp. 16927–16936, Aug. 2021, doi: 10.1109/JSEN.2021.3078512.

[57] L. Tonin et al., "Learning to control a BMI-driven wheelchair for people with severe tetraplegia," *iScience*, vol. 25, no. 12, Dec. 2022, Art. no. 105418, doi: 10.1016/j.isci.2022.105418.

[58] D. Forenzo, H. Zhu, J. Shanahan, J. Lim, and B. He, "Continuous tracking using deep learning-based decoding for noninvasive brain–computer interface," *PNAS Nexus*, vol. 3, no. 4, p. 145, Apr. 2024, doi: 10.1093/pnasnexus/pgae145.